ORNL/SPR-2024/3426
Rev. 0

Report on RIA Relevant Modified Burst Testing of ATF Cladding Materials

Nuclear Technology Research and Development

Prepared for
US Department of Energy
Nuclear Technology R&D
Advanced Fuels Campaign

Authors:
M Nedim Cinbiz, Benton Garrison,
Kory Linton
Oak Ridge National Laboratory

June 2024
M3FT-24OR020204044

ACKNOWLEDGMENTS

This research was sponsored by the Advanced Fuels Campaign Program of the US Department of Energy (DOE) Office of Nuclear Energy. The report was authored by UT-Battelle LLC under Contract No. DE-AC05-00OR22725 with DOE.

SUMMARY

The mechanical performance of accident-tolerant fuel (ATF) cladding candidates in light-water reactors (LWRs) must be similar to or better than that of current conventional nuclear fuel claddings to reduce dose to the public and ensure a that the core coolable geometry is maintained during a postulated reactivity-initiated accident (RIA) in light-water reactors (LWRs). During an RIA event, the rapid thermal expansion of nuclear fuel can deform the cladding once the fuel–cladding gap closes. In some cases, the pellet–cladding mechanical interaction (PCMI) can induce mechanical failure in ATF candidates. Thus, the mechanical response of ATF cladding must be investigated by mimicking the conditions of RIA and potentially performing Transient Reactor Test (TREAT) experiments to establish or verify the safety envelope.

The work presented in this report investigated the failure behavior of as-received, hydrided, and chromium-coated (Cr-coated) Zircaloy-4 (Zry-4) cladding tube under strain-driven mechanical conditions, mimicking postulated RIA loading conditions. Mechanical testing was performed at 300°C via modified burst test (MBT) equipment with pulse width control previously developed under the Department of Energy's (DOE's) Advanced Fuel Campaign (AFC). The mechanical strains were determined using 2D digital image correlation (DIC) techniques. The base Zry-4 acquired by Cameco Inc. was in stress-relieved annealed (SRA) condition. Because of the observed large deformation of the cladding tubes, the failure strain definition was updated for the MBT, which can also be applied to other tube tests where significant bulging (out-of-plane deformation) is present. The failure strain was determined to be affected by the speed of the test or the RIA event. As the RIA-like event duration decreased from 75 to 15 ms, the failure strain decreased 5, 7 and 1% for as-received, hydrided, and Cr-coated specimens, respectively. Fractography on the Cr-coated specimens indicated the presence of two failure mechanisms: (i) crenulation at the outer surface of the coating due to the tensile tractional forces along with coatings grain microstructure and (ii) formation of critical defect at the coating/cladding interface that initiated coating rupture after severe plastic deformation of the Zry-4 substrate.

Based on the MBT results and fractography observations, performing mechanical property testing at high strain rates—in particular on Cr-coated tubes—and semi-integral TREAT experiments are required future efforts to ensure ATF cladding performance during transients. The testing recommended would also inform the development of long-term generalized cladding technologies.

CONTENTS

FIGURES

TABLES

ACRONYMS

Acronym	Description
AFC	Advanced Fuels Campaign
AR	as received
ATF	accident-tolerant fuel
ATT	axial tensile test
CWSR	cold-worked stress-relieved
DIC	digital image correlation
DOE	US Department of Energy
EDC	expansion due to compression
HIPIMS	high-power impulse magnetron sputtering
LOCA	loss-of-coolant accident
MBT	modified burst test
PCMI	pellet–cladding interaction
PST	plane strain tension
RIA	reactivity-initiated accident
RTT	ring tensile test
SEMT	segmented mandrel test
SRA	stress-relieved annealed
Zry-4	Zircaloy-4

REPORT ON RIA RELEVANT MODIFIED BURST TESTING OF ATF CLADDING MATERIALS

1. INTRODUCTION

The mechanical performance of accident-tolerant fuel (ATF) cladding candidates must demonstrate similar to or better performance than the conventional light-water reactor (LWR) cladding under postulated transient conditions [1-3]. Although ATF development mainly focuses on loss-of-coolant accident (LOCA) and severe accident conditions [4, 5], the mechanical integrity of the nuclear fuel cladding must be ensured during steady-state and other postulated accidents such as reactivity-initiated accidents (RIA) in LWRs [2, 6]. During the RIA, occurrence of a postulated control rod ejection triggers a prompt increase of the fission rate density [2, 7-9]. The energy deposition, as correlated with the fission rate density, yields a significant fuel temperature increase and subsequent isotropic thermal expansion of fuel in milliseconds. While the negative temperature feedback scrams the reactor, the fuel expansion can drive the cladding to biaxially deform if the two are in contact, so-called *pellet–cladding mechanical interaction* (PCMI). Importantly, the irradiated cladding may fail during the PCMI phase, as manifested by the cladding strength, ductility, and amount of the deposited energy [9]. Therefore, assessment of the PCMI phase of RIA is critical in determining the safe design limits for ATF candidates.

Integral tests provide an ultimate assessment of fuel and cladding for the development of validation cases and characterization of the consequences on the components after transients. However, these tests' effectiveness is low in terms of extracting the essential mechanistic effects to develop material models for fuel performance codes to determine the design-basis margins for transients [2]. Therefore, major safety research programs—like those that used the NSSR and CABRI reactors—include separate effects testing to capture the phenomena-specific conditions and to perform material property determination for establishing the safety envelope and novel material selection rules without taking up scarce space in research reactors[10-14].

Multiple mechanical testing techniques have been developed to study the fuel-driven deformation of cladding in a manner that mimics phenomena-specific conditions such as iodine-induced stress corrosion cracking, load-following, and the PCMI phase of RIA [15-17]. Whereas actual PCMI conditions are complex and affected by fuel cladding bonding status, fuel-to-cladding surface friction, cladding microstructure, biaxial strength of the cladding, and localized microstructural features [14], all separate effects tests aim to simulate the fuel-imposed complex tractions and loading rates on the cladding inner surface [14, 16].

In segmented expanding mandrel tests (SEMTs), the mandrel lateral displacement causes specimen deformation [15, 18]. During SEMTs, the specimen experiences tension, bending, and compression fields along the hoop direction [18]. If failure is not confined to the hoop tension zone in SEMT, then specimen failure can occur at an unfavored stress magnitude and stress biaxiality. On the other hand, expansion due to compression (EDC) tests resolve the non-uniform stress along the hoop direction imposed by SEMT by using a soft cylindrical (polyurethane or aluminum) plug that expands while it is compressed during the test [17, 19]. In principle, the expanding plug forces the cladding to uniformly deform along the hoop direction. One shortcoming of EDC testing for highly-ductile specimens is that the expanding region gets smaller as the soft plug is compressed, which localizes the hoop deformation to a small strip of material in the axial direction, effectively reducing the gauge size during the test. While this localized hoop deformation may mimic specific traction conditions such as isotropic expansion of a fuel pellet during RIA, the mechanical strain path can be remedied by modified EDC tests using fixed-end tubes or tensile loading [17, 19]. Alternatively, the plane strain tension (PST) test aims to address the mechanical strain path challenge of mimicking RIA-type conditions by using a notched gauge section where the central section of the specimen

experiences a near biaxial strain state [20]. Similar to SEMT, PST specimens suffer from non-uniform loading condition such that specimen failure can initiate at the notch roots where the loading path is uniaxial tensile rather than biaxial.

To address some of the shortcomings of strain-driven tests, the modified burst test (MBT) concept was initially designed to simulate the strain-driven rapid loading conditions experienced by the fuel cladding experiences during the PCMI phase of a LWR RIA event [2, 21]. As compared to other strain-driven tests such as SEMT, EDC, and PST, the relatively large region of the specimens, corresponding to one fuel pellet length, is uniformly deformed under PST via internal pressurization of another tube (i.e., a driver tube) at high speeds. This enables MBT to investigate the cladding's rupture behavior under RIA-like loading conditions, providing a unique advantage over other strain-driven tests. In general, MBT is a mechanical behavior performance test that is used for (1) go/no-go decision-making based on the cladding rupture behavior, (2) initial safety design parameter determination for integral tests, (3) unraveling the failure characteristics of novel cladding components, and (4) fuel performance code validation/confirmation.

This report presents MBT tests performed at 300°C on as-received (AR), hydrided, and Cr-coated Zircaloy-4 (Zry-4) specimens at different internal pressurization rates corresponding to different RIA event times. MBT tests utilized optical metrology and digital image correlation (DIC) techniques to estimate the mechanical strain. To overcome shortcomings related to the determination of failure strain caused by bulging (out-of-plane deformation), the minimum failure strain concept was introduced to represent the failure strain in strain-driven mechanical tests like the MBT. Specific attention was given to the failure behavior of Cr-coated cladding tubes via fractography. The results emphasize the importance of targeted integral testing at the Transient Reactor Test (TREAT) Facility reactor with the required separate effects testing support for accurate fuel performance modeling.

2. MATERIALS AND METHODS

2.1 TUBE SPECIMENS

This study used Zry-4 tubing with equiaxed alpha zirconium grains as the base material from Cameco Fuel Manufacturing (Port Hope, Ontario, Canada). The average grain size was determined as 5–10 μm. This base material was subjected to Cr coating or a hydriding process to investigate the impact of coating or hydrides on the failure behavior. Chromium coating was performed using physical vapor deposition by way of the high-power impulse magnetron sputtering technique (HIPIMS) [22, 23]. A dense 6 to 9 μm thick Cr coating was applied to the Zry-4 tubes. Before coating, the surface of the tubes was polished by APEX grinding to reduce the surface roughness, which improved the coating adherence.

Coating microstructure consisted of elongated columnar Cr grains that were grown outward from the cladding outer surface along the radial direction. The uniformity of the Cr–Zry4 interface was dependent on the outer surface condition of the Zry-4 tubes, and their surface roughness was reduced by mechanical polishing.

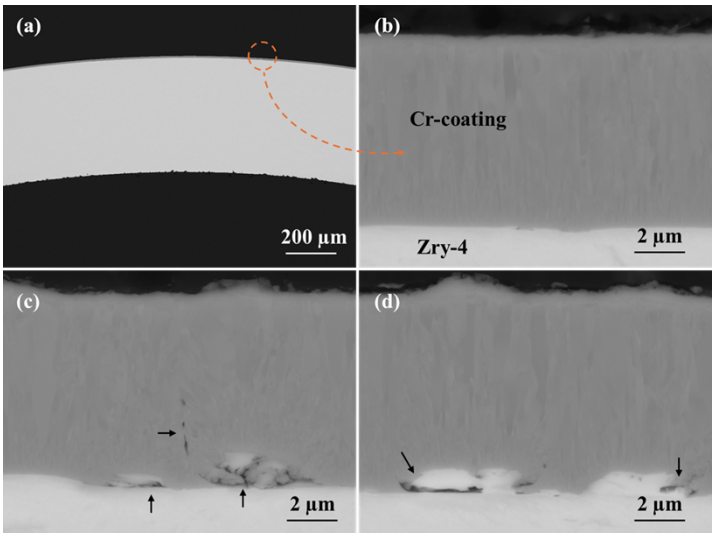

Figure 1 (a) Coated cladding microstructures showing (b) a proper coating adhesion, (c) macroscopic defects in the coating, and (d) interface defects.

Hydriding was performed in a static chamber via gaseous diffusion of hydrogen. The chamber was initially vacuumed down to 13.33 µPa (10^{-7} Torr) and sealed at that pressure prior to introducing pure H_2 gas into the chamber at ambient temperature. Then, the chamber was heated up to 525°C, at which the chamber was soaked for 4–6 hours. This step was also expected to yield some additional stress relieving on the cladding tubes. After hydriding, the H of the specimens was measured via a standard inert gas fusion process. The specimens were hydrided to levels ranging from 300 to 500 wt. ppm of hydrogen.

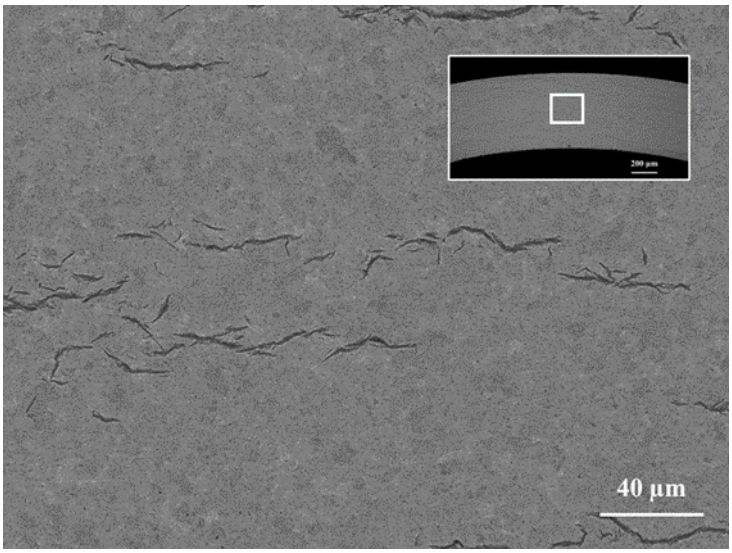

Figure 2 Representative hydrided cladding microstructure (~300 wt. ppm of H).

To enable comparison with the MBT results, baseline mechanical tests were performed on AR, Cr-coated, and hydrided specimens. Mechanical test specimens were machined to the axial and ring tensile (ATT and RTT) geometries shown in Figure 6 using end mill machining. Crosshead displacement-

controlled tests were performed at a nominal strain rate of ~1 × 10^{-3} s^{-1} using an Instron 5966 with a resistance-heated clamshell furnace. Specimen types and major mechanical test results are listed in Table 1. In general, all specimens exhibited significant elongation above 35% at 300°C. Mechanical softening effects in both yield and ultimate tensile stress values were observed for the hydrided specimens as compared to the AR specimens. Hydrided specimens tested via ATT and RTT had higher H content compared to that of their MBT counterparts (~300 wt. ppm) due to the specimen availability. However, the H content's impact on the overall mechanical behavior was expected to be insignificant with the range of 300–600 wt. ppm at 300°C based on the relevant literature [24-26].

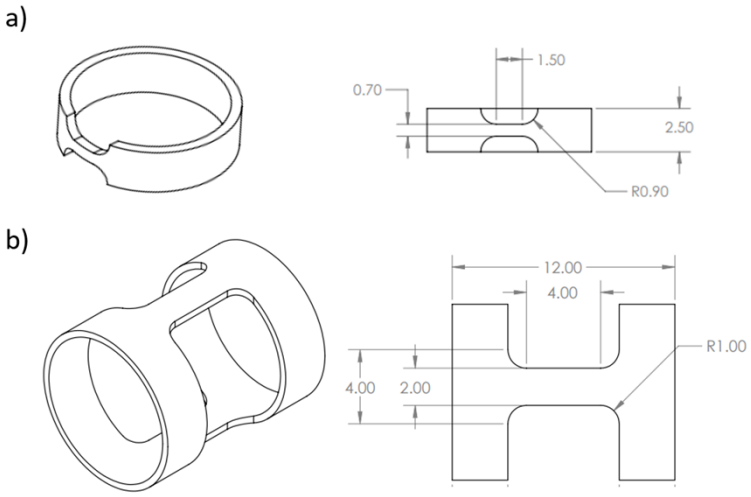

Figure 3 Drawings of (a) RTT and (b) ATT specimens used in this work. All dimensions are in millimeters.

Table 1 Hoop and axial tension results of as-received, Cr-coated, and hydrided specimens for baseline estimations. UTS stands for the ultimate tensile strength, *Total elongations determined after removing elastic displacement, calculated from the apparent modulus of the material from the mechanical test data

Specimens type	Test type	Temperature (°C)	Hydrogen content (wt.ppm)	0.2% Yield stress (MPa)	UTS (MPa)	Total elongation* (%)
As-received	Axial tension	300	0	250	371	35.3
As-received	Hoop tension	300	0	365	412	49.4
Cr-Coated	Axial tension	300	0	281	410	31.5
Cr-Coated	Hoop tension	300	0	379	418	43.7
Hydrided	Axial tension	300	543	179	279	55.6
Hydrided	Hoop tension	300	543	220	312	65.4

2.2 MODIFIED BURST TEST AND OPTICAL METROLOGY

The MBT is an indirect mechanical test in which the open-ended cladding tube is deformed by an expansion of another high-strength closed-end tube made of age-hardened Inconel 718 with complex interior geometry (driver tube) [2, 21]. The driver tube internal geometry consists of a one-fuel-pellet-long thin-wall region that drives the specimen deformation (see Figure 4) via internal pressurization. In contrast with previous MBT testing, the tube specimen was sleeved onto the driver tube via shear-fitting or with a ceramic glue. The driver tube was pressurized by compression of high-temperature stable (up to 350°C) hydraulic oil (Krytox XHT-500) via volume reduction of a piston chamber connected to the driver tube at high-speeds to mimic RIA-imposed loading rates. Loading rate is controlled by the speed of the actuator, which affects the speed of volume reduction inside the piston chamber and thus the pressurization rate.

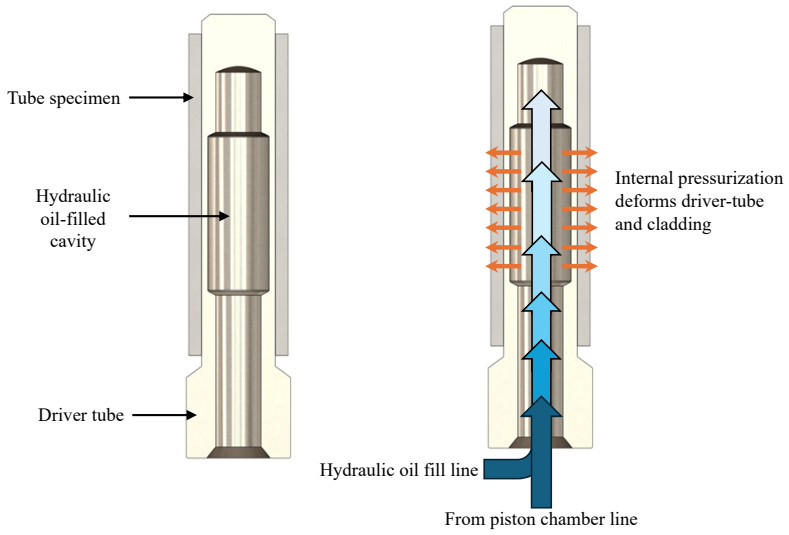

Figure 4 Schematic of the MBT without core-pin arrangement.

Mechanical strains were measured with optical metrology and DIC techniques. Optical metrology benefited from the first surface mirror arrangement to acquire a 360°-view of the specimens with four projections, which were acquired by an ultra-high-speed camera (Photron AX-200) through a telecentric lens (see Figure 5) [1]. The high frame rates enabled the determination of the moment when fracture occurred, and the large field of view enabled the determination of fracture location. Accommodating for the large field of view resulted in a resolution of ~68 µm/pixel.

Two-dimensional DIC was employed to calculate the mechanical strains using a custom in-house software that was previously assessed for MBT and other mechanical tests [1]. For DIC calculations, subset sizes of 63 pixel width squares were used, based on a previous DIC assessment. Because the optical metrology setup utilized a telecentric lens, which captures orthogonal projections, all parallax was minimized. As a result of 2D DIC, the out-of-plane deformation associated with deformation in the cylindrical coordinates and ballooning was analyzed as in-plane deformation. This was expected to deviate the DIC strain values by 0.075% if the actual (prescribed) hoop strain was 20% [1].

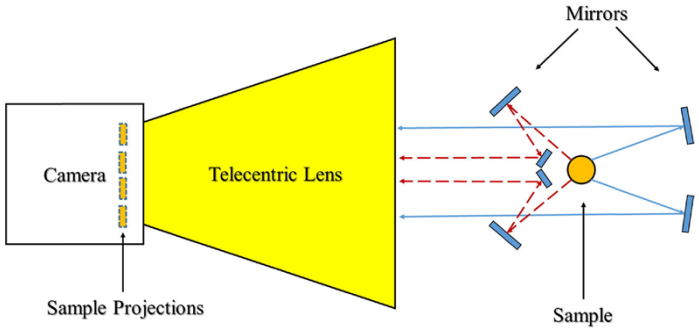

Figure 5 Schematics of the optical metrology system [1].

2.3 FAILURE STRAIN ASSESSMENT FOR MODIFIED BURST TEST

The determination of the mechanical strain is the essence of the failure and rupture assessment of the cladding tubes that are subjected to out-of-plane deformation whereby the axisymmetric uniformity is lost, as observed in actual reactor transients (LOCA and RIA) and separate effects tests (burst, MBT, EDC, and SEMT). For internal pressurization conditions, most of the studies use diametral strain measurements, whether or not 2D optical metrology is available. This approach is efficiently translated into the hoop strain for the uniform plastic deformation of the tubing. By exceeding the uniform plastic deformation, the diametral strain measurement inherently averages all non-uniformity caused by localized bulging, and additional metrics for the rupture region are needed to assess the mechanical strain, such as those measured in post-LOCA tests [3, 27].

For strain-driven out-of-plane deformation conditions (MBT, EDC, and SEMT), the determination of a failure criterion is critical because the plastic deformation is localized to specific spatial coordinates on the specimen where other regions do not deform. Previous MBT studies have aimed to locate the spatial location of the fracture with high-speed optical metrology to determine the failure strain close to the rupture moment. This approach provided insights to evaluate the cladding performance from the core coolable geometry perspective during a postulated RIA [6, 28].

In fact, burst tests on driver tubes (internal pressurization) have indicated that the DIC-measured strain ranges from approximately 5% to 17% at different hoop locations, where the highest value has corresponded to the rupture location [1]. If specimens exhibit low ductility, then the variations on the strain will be lower over the specimen's spatial coordinates. However, specimens that deform at higher ductility can experience a significant non-uniform bulging, in particular for MBT. For instance, Figure 6 depicts the significant nonuniformity of 2D DIC-measured strain distribution on the specimen surface, which ranges from ~0.07 (7%) to ~0.17 (17%). Thus, the definition of failure strain needs to be revisited for out-of-plane deforming specimens at large strains if there is no optical metrology capability or optical metrology limited to 2D.

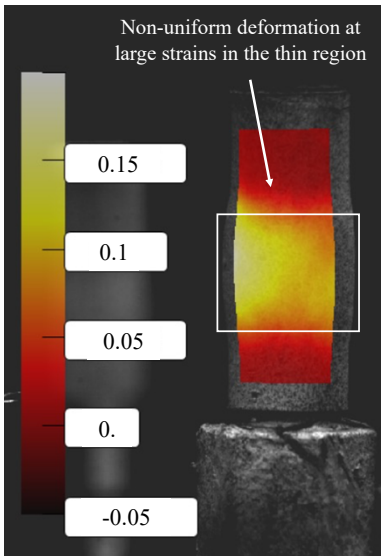

Figure 6 Depiction of non-uniform strain distribution observed in AR specimens (the first principal strain corresponds to diametrical strain) during MBT test (frame was taken right at the failure moment).

This study applied a minimum failure strain definition for MBT by adapting the limit strain concept [29]. The minimum value of the 2D DIC-measured first principal strain immediately before the rupture moment was accepted as the failure strain at which the uniform deformation was exceeded during the test. Beyond this strain value, the specimen continued to deform in a localized manner. Therefore, strain values at the deforming region of the specimen during the test at different projections were compared, and the lowest value was picked as the minimum failure strain in this work. Although this approach adds more conservatism to the results, it practically addressed the strain determination challenge during strain-driven tests like the MBT.

3. RESULTS AND DISCUSSION

3.1 MBT RESULTS AND MINIMUM FAILURE STRAIN

Figure 7 shows typical MBT test data for an AR Zry-4 specimen (240209-1) tested at a rate of 127 mm/s. For the specific test, the driver tube was filled to 50 MPa of oil pressure prior to test start. With the start of the test, the internal pressure of the driver tube increased, as did the 2D DIC-calculated strain, until specimen rupture occurred. The initial fluctuation of the strain was likely caused by the rapid pressurization-induced vibrations.

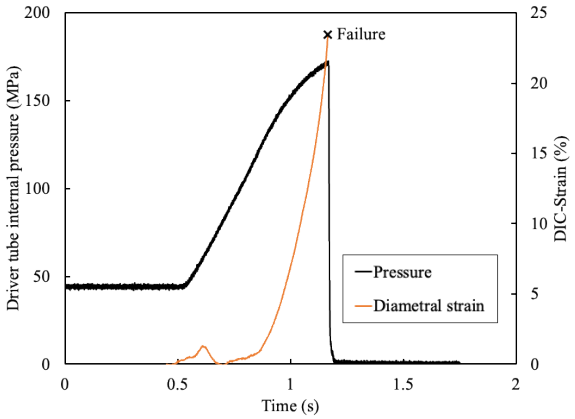

Figure 7 A typical MBT internal pressure and DIC strain measurement data (AR specimen that was loaded at 127 mm/s).

Figure 8 shows the selected picture frames of 360° view of the Cr-coated Zry-4 specimen (240306-1) and map of DIC-calculated strain on the ruptured surface. At the beginning of the test, the DIC-measured strain was zero. As the test started, the specimen expanded due to driver tube expansion. The picture frame just before the rupture indicated a significant localized deformation in the thin section up to 0.125 (12.5%). At this frame, the DIC software also lost tracking of some regions in the maps, and by the last frame—at which the mechanical rupture occurred—all maps were completely off-track.

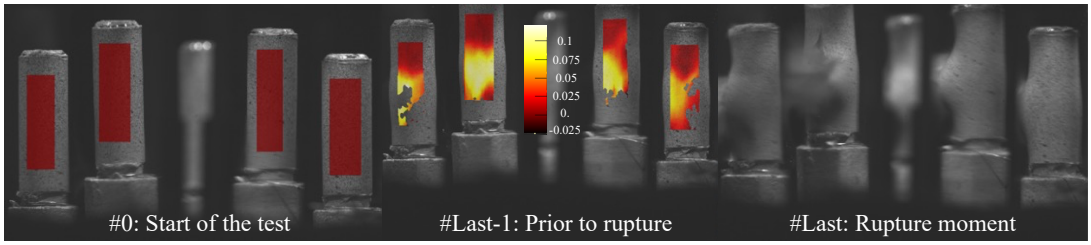

Figure 8 optical metrology and DIC map on the rupture surface

Figure 9 shows the minimum and maximum strains as determined prior to the rupture moment (see Table 2 below) as a function of the MBT loading rate. The DIC-measured minimum strain was used as the failure strain criteria. The minimum failure strain of all type of specimens showed a dependency on the loading rate. As the MBT test speed increased from 127 to 762 mm/s, the minimum failure strain of AR specimens decreased from ~13.22% to ~8.96%—almost 5%. Hydrided specimen exhibited a similar behavior where the minimum failure strain decreased from ~14.27% to 7.81%. A slight decrease in the minimum failure strain (from ~4.97% to ~3.1%) was also determined for Cr-coated specimens as the MBT test speed increased from 25.4 to 762 mm/s. Hydrided specimens were not tested at very high speeds due to equipment availability. When compared with RTT and ATT tests, all MBT specimens showed lower failure strains. This result is attributed to the higher biaxiality ratios and [29] and the presence of hoop direction confinement during the tests.

Noticeably, the DIC-measured minimum and maximum failure strains exhibited ~5% strain variation for Cr-coated specimens. Furthermore, the maximum failure strains were similar for Cr-coated specimens tested at 25.4 and 762 mm/s and the AR specimen that was tested at 762 mm/s. This indicated that the ultimate rupture of the cladding was controlled by the Zry-4 substrate: Cr coating had limited impact, and cracking of the Cr coating was also observed as crenulation. However, this behavior could cause secondary consequences for fuel cladding safety because potential coating cracking would accelerate hydrogen pick-up or localized oxidation during reactor startups and shutdowns or load-following.

Table 2 List of MBT experiments

Sample	Temperature (°C)	Speed (mm/s)	Corresponding RIA event time (ms)	Coated	H (ppm)	Minimum strain (%)	Maximum strain (%)
240227-1	300	127	~75	No	300	14.93	18.81
240215-3	300	25.4	~700	No	300	14.27	19.36
240624-1*	300	762	~15	No	300	7.81	8.64
240209-1	300	127	~75	No	0	13.22	17.20
240129-1	300	762	~15	No	0	8.96	9.50
240306-1	300	25.4	~700	Yes	0	4.97	9.10
240307-1	300	762	~15	Yes	0	3.1	9.25

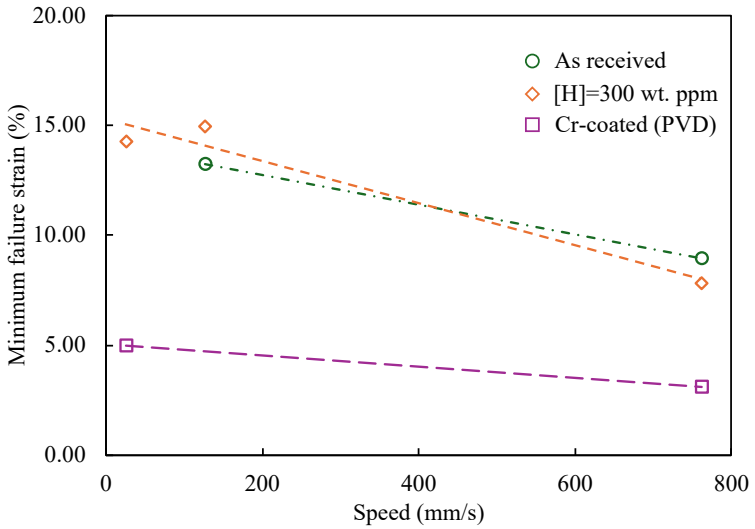

Figure 9 Minimum failure strain of the AR, hydrided, and coated specimens as a function of MBT loading rate.

Figure 10 shows typical rupture surfaces observed for the AR, hydrided, and Cr-coated specimens. AR and hydrided specimens exhibited large diametrical expansion, but no axial split was determined as expected from the cold-worked stress-relieved (CWSR) specimens. This result is attributed to the grain microstructure difference of the Cameco Zry-4. For the Cr-coated specimens, the hoop expansion was limited, and axial crack propagation was observed. Although all specimens failed in a ductile manner, special attention to Cr coating rupture behavior was given because the minimum failure strain was very low for the coated specimens.

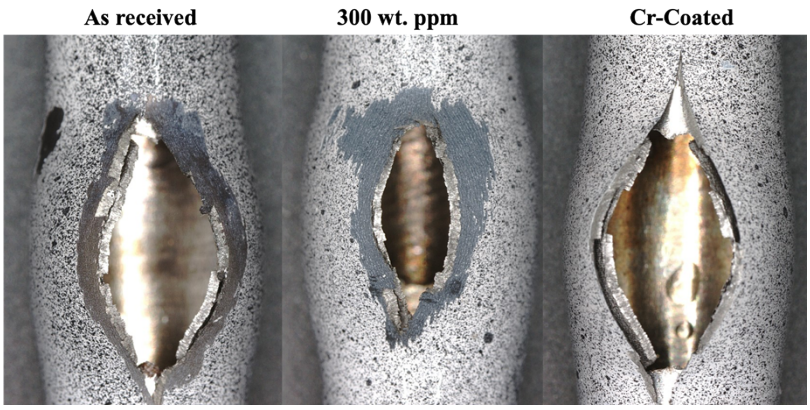

Figure 10 Descriptive images of the failed specimens after MBT test.

3.2 FRACTURE SURFACE ANALYSIS OF CR-COATED SPECIMENS

Figure 11 shows (a) the overall fracture surface of failed Cr-coated specimens and (b) the high magnification SEM image. Fractography indicated that significant ductile damage accumulated in the Zry-4 substrate, whereas the Cr coating exhibited negligible void-like features because of mechanical damage. This also revealed that the significant plastic deformation was accommodated in the soft Zry-4 substrate until the hard Cr coating ruptured. Thus, the overall diametral expansion was limited because the hard Cr-coating confined the Zry-4 substrate's ability to deform. Important features that led the coating failure were initiated at the coating–substrate interface, as indicated by asterisk symbol (*) in Figure 11(b). No apparent coating delamination was observed in all samples, which confirmed high adherence to substrate. However, coating crenulation was observed, which further led to coating tensile failure without delaminating from the Zry-4 substrate. Because DIC paint avoided to obtain high-quality pictures from the crenulated surface, the coating failure characteristics were shown using RTT specimen rupture surface (see Figure 12), where Cr coating rupture was clear in the inset pictures. The major coating separation was observed perpendicular to the tensile load direction, and minor longitudinal cracks were also present.

Overall, the main failure mechanism consisted of severe plastic deformation of Zry-4 where Cr coating scaling-off occurred. Whereas no delamination from the Zry-4 was observed, the Cr coating separation was governed by the coating's limited ductility and tensile forces. The major responsible mechanisms for the coating cracking were: (i) the void nucleation at the substrate–coating interface during the plastic deformation. As voids grew to a critical size due to void growth and coalescence, the stress intensity at a particular location reached the tensile strength value of the coating, (ii) crenulation at the coating outer surface, which was controlled by the tensile surface tractions and coating grain microstructure. The main controlling failure mechanism was still ductile processes of void initiation, growth, and coalescence at the component level. The coating crenulation may be critical for nuclear fuels subject to environmental degradation under cyclic conditions or anticipated operational transients. Such crenulated regions, if present, during reactor operation may yield hydrogen pick-up and oxidation, which may degrade the postulated transient behavior of coated claddings.

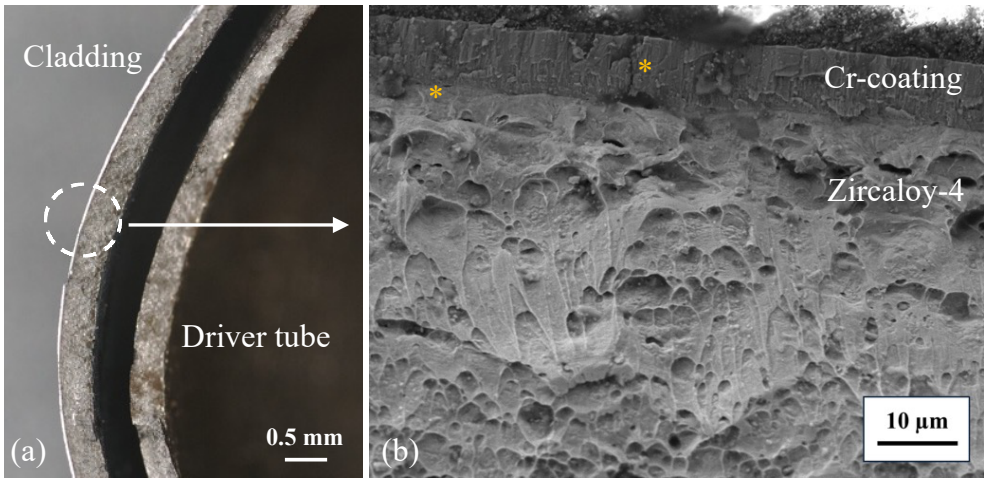

Figure 11 Fracture surface of MBT-tested Cr-coated specimen (a) low-magnification optical image and (b) SEM image of Cr coating–Zry-4 interface. Asterisks (*) indicate selected important commonly observed features of the fracture surface.

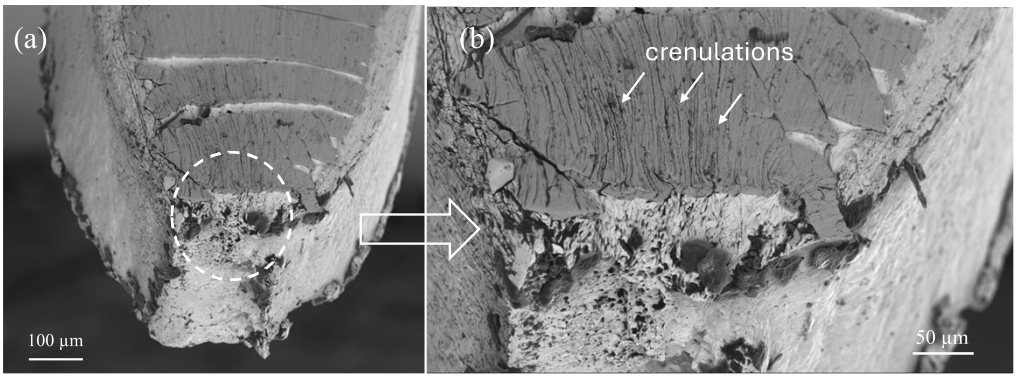

Figure 12 SEM micrographs of the fracture surface of RTT-tested Cr-coated specimen at (a) low and (b) high magnifications.

4. SUMMARY AND FUTURE DIRECTIONS

The work documented in this report investigated the failure behavior of AR, hydrided, and coated Zry-4 cladding tube under strain-driven mechanical conditions, mimicking postulated RIA loading conditions. The base Zry-4 was provided by Cameco Inc. in stress-relieved annealed condition, which was softer than conventional CWSR Zry-4. The main takeaways are as follows:

i. The assessment of the failure strain with 2D DIC was updated for the ductile tube specimens for which out-of-plane deformation is non-negligible. The approach used in the work imposed additional conservatism to the definition of the failure strain as determined by a 2D DIC technique.

ii. The minimum failure strain decreased with increasing test speed, from 25.4 to 732 mm/s (or RIA event-time from 75 to 15 ms, respectively), for AR, hydrided (300 wt. ppm), and Cr-coated Zry-4 cladding. This result indicates the importance of determination of strain-rate effects on the mechanical properties of cladding tubes and their implementation in fuel performance codes for TREAT tests.

iii. A unique failure behavior was observed in Cr-coated specimens. The delamination of coating from the substrate was insignificant even at severe deformations: the plastic strains were up to 40%, as

observed in RTT and ATT. The failure of the Cr coating included (i) crenulation at the coating outer surface, which was controlled by the tensile surface tractions and coating grain microstructure, and (ii) critical defect formation at the coating–substrate interface due to the void initiation, growth, and coalescence processes. The main controlling failure mechanism was still ductile processes of void initiation, growth, and coalescence.

The results presented in this report indicate the impact of the strain rate effect on cladding tube deformation during RIA transients and future TREAT integral tests. Importantly, the Cr-coated tube failure behavior suggested that the coating crenulation may be critical for nuclear fuels subject to environmental degradation under cyclic conditions or anticipated operational transients. Such crenulated regions, if present, during reactor operation may yield hydrogen pick-up and oxidation, which may degrade the postulated transient behavior of coated claddings. To ensure the safety of ATF cladding, the following future work is suggested: (i) determination of strain rate effects on the mechanical properties, particularly for coated ATF cladding candidates, (ii) design of semi-integral tests for TREAT reactor with specimen preconditioning at the High Flux Isotope Reactor to simulate extended burnup conditions, and (iii) establishing widely accepted failure strain determination procedures for out-of-plane deformation as commonly observed in postulated transients.

5. REFERENCES

1. Cinbiz, M.N., et al., *An advanced experimental design for modified burst testing of nuclear fuel cladding materials during transient loading.* Annals of Nuclear Energy, 2019. **127**: p. 30-38.
2. Cinbiz, M.N., et al., *A pulse-controlled modified-burst test instrument for accident-tolerant fuel cladding.* Annals of Nuclear Energy, 2017. **109**: p. 396-404.
3. Garrison, B., et al., *Burst characteristics of advanced accident-tolerant FeCrAl cladding under temperature transient testing.* Journal of Nuclear Materials, 2022. **560**: p. 153488.
4. Zinkle, S.J., et al., *Accident tolerant fuels for LWRs: A perspective.* Journal of Nuclear Materials, 2014. **448**(1): p. 374-379.
5. Terrani, K.A., *Accident tolerant fuel cladding development: Promise, status, and challenges.* 2018.
6. Cinbiz, M.N., et al., *Failure behavior of SiC/SiC composite tubes under strain rates similar to the pellet-cladding mechanical interaction phase of reactivity-initiated accidents.* Journal of Nuclear Materials, 2019. **514**: p. 66-73.
7. Ishikawa, M. and S. Shiozawa, *A study of fuel behavior under reactivity initiated accident conditions — review.* Journal of Nuclear Materials, 1980. **95**(1): p. 1-30.
8. Fuketa, T., H. Sasajima, and T. Sugiyama, *Behavior of High-Burnup PWR Fuels with Low-Tin Zircaloy-4 Cladding under Reactivity-Initiated-Accident Conditions.* Nuclear Technology, 2001. **133**(1): p. 50-62.
9. Wilson, G.E. and B.E. Boyack, *The role of the PIRT process in experiments, code development and code applications associated with reactor safety analysis.* Nuclear Engineering and Design, 1998. **186**(1): p. 23-37.
10. Nagase, F., T. Sugiyama, and T. Fuketa, *Optimized ring tensile test method and hydrogen effect on mechanical properties of zircaloy cladding in hoop direction.* Journal of nuclear science and technology, 2009. **46**(6): p. 545-552.
11. Nagase, F. and T. Fuketa, *Investigation of Hydride Rim Effect on Failure of Zircaloy-4 Cladding with Tube Burst Test.* Journal of Nuclear Science and Technology, 2005. **42**(1): p. 58-65.
12. Cazalis, B., et al., *The PROMETRA Program: Fuel Cladding Mechanical Behavior under High Strain Rate.* Nuclear Technology, 2007. **157**(3): p. 215-229.
13. Balounlet, M., et al., *The Prometra programme: assessment of mechanical properties of zircaloy 4 fuel cladding during an RIA.* 1999.

14. Leclercq, S., A. Parrot, and M. Leroy, *Failure characteristics of cladding tubes under RIA conditions.* Nuclear Engineering and Design, 2008. **238**(9): p. 2206-2218.
15. Nobrega, B.N., et al., *The influence of localized stresses and strains on the iodine scc behavior of Zircaloy-2 tubing.* Journal of Nuclear Materials, 1985. **131**(2): p. 126-135.
16. Desquines, J., et al., *The issue of stress state during mechanical tests to assess cladding performance during a reactivity-initiated accident (RIA).* Journal of Nuclear Materials, 2011. **412**(2): p. 250-267.
17. Hellouin de Menibus, A., et al., *Fracture of Zircaloy-4 cladding tubes with or without hydride blisters in uniaxial to plane strain conditions with standard and optimized expansion due to compression tests.* Materials Science and Engineering: A, 2014. **604**: p. 57-66.
18. Nilsson, K.-F., et al., *The segmented expanding cone-mandrel test revisited as material characterization and component test for fuel claddings.* Nuclear Engineering and Design, 2011. **241**(2): p. 445-458.
19. Zouari, A., et al., *The effect of strain biaxiality on the fracture of zirconium alloy fuel cladding.* Journal of Nuclear Materials, 2021. **554**: p. 153070.
20. Link, T.M., D.A. Koss, and A.T. Motta, *Failure of Zircaloy cladding under transverse plane-strain deformation.* Nuclear Engineering and Design, 1998. **186**(3): p. 379-394.
21. Yueh, K., *Applicability of modified burst test data to reactivity initiated accident.* Journal of Nuclear Materials, 2017. **488**: p. 338-345.
22. Graening, T., et al., *Microstructure Investigation and Mechanical Properties of Coated Zircaloy Cladding*. 2021: United States. p. Medium: ED; Size: 31 p.
23. Le Coq, A., et al., *AFC FY 2023 HFIR Irradiation Test Matrix – Supported by the Design of a Ring Specimen Irradiation Vehicle*. 2023: United States. p. Medium: ED; Size: 25 p.
24. Le Saux, M., et al., *Behavior and failure of uniformly hydrided Zircaloy-4 fuel claddings between 25°C and 480°C under various stress states, including RIA loading conditions.* Engineering Failure Analysis, 2010. **17**(3): p. 683-700.
25. Cinbiz, M.N., *The effect of stress state on zirconium hydride reorientation*. 2015, The Pennsylvania State University: United States -- Pennsylvania. p. 218.
26. Arsene, S., J.B. Bai, and P. Bompard, *Hydride embrittlement and irradiation effects on the hoop mechanical properties of pressurized water reactor (PWR) and boiling-water reactor (BWR) ZIRCALOY cladding tubes: Part I. Hydride embrittlement in stress-relieved, annealed, and recrystallized ZIRCALOYs at 20 °C and 300 °C.* Metallurgical and Materials Transactions A, 2003. **34**(3): p. 553-566.
27. Garrison, B., et al., *Length Dependence of Severe Accident Test Station Integral Testing*. 2019, ; Oak Ridge National Lab. (ORNL), Oak Ridge, TN (United States). p. Medium: ED.
28. Brown, N.R., et al., *Mechanical failure of fresh nuclear grade iron–chromium–aluminum (FeCrAl) cladding under simulated hot zero power reactivity initiated accident conditions.* Journal of Nuclear Materials, 2020. **539**: p. 152352.
29. Yunchang, F. and D. Koss, *The influence of multiaxial states of stress on the hydrogen embrittlement of zirconium alloy sheet.* Metallurgical Transactions A, 1985. **16**(4): p. 675-681.